Optimal operating parameters for advanced alkaline water electrolysis

Available online at www.sciencedirect.com

ScienceDirect

journal homepage: www.elsevier.com/locate/he

Optimal operating parameters for advanced alkaline water electrolysis

Matheus T. de Groot [a,b,*], *Joost Kraakman* [a], *Rodrigo Lira Garcia Barros* [a]

[a] *Eindhoven Institute for Renewable Energy Systems, Eindhoven University of Technology, P.O. Box 513, 5600 MB Eindhoven, the Netherlands*

[b] *HyCC, Van Asch van Wijckstraat 53, 3811 LP Amersfoort, the Netherlands*

HIGHLIGHTS

- A nominal current density of 1.8 A cm^{-2} seems achievable for alkaline electrolysis.
- To enable a minimum load of 10%, the pressure is preferably kept below 8 bara.
- Gas crossover is mainly driven by diffusive hydrogen transport.
- Supersaturation at the diaphragm interface plays an important role.

GRAPHICAL ABSTRACT

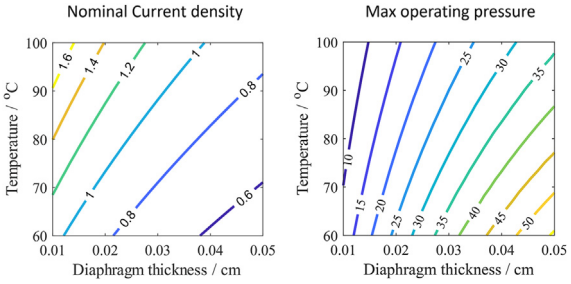

ARTICLE INFO

Article history:
Received 9 February 2022
Received in revised form
22 July 2022
Accepted 7 August 2022
Available online 6 September 2022

Keywords:
Alkaline electrolysis
Nominal current density
Cell potential
Gas crossover
Supersaturation
Diaphragm

ABSTRACT

Advanced zero-gap alkaline electrolyzers can be operated at a significantly higher current density than traditional alkaline electrolyzers. We have investigated how their performance is influenced by diaphragm thickness, temperature and pressure. For this a semi-empirical current-voltage model has been developed based on experimental data of a 20 Nm^3/h electrolyzer. The model was extrapolated to thinner diaphragm thicknesses and higher temperatures showing that a nominal current density of 1.8 A cm^{-2} is possible with a 0.1 mm diaphragm at 100 °C. However, these operating parameters also lead to increased gas crossover, which limits the ability to operate at low loads. A gas crossover model has been developed, which shows that crossover is mainly driven by diffusive transport of hydrogen, caused by a high local supersaturation at the diaphragm surface. To enable a low minimum load of 10% the operating pressure should be kept below 8 bara.

* *Corresponding author*. Eindhoven Institute for Renewable Energy Systems, Eindhoven University of Technology, P.O. Box 513, 5600 MB Eindhoven, the Netherlands.
E-mail address: M.T.d.Groot@tue.nl (M.T. de Groot).

https://doi.org/10.1016/j.ijhydene.2022.08.075

Introduction

Green hydrogen produced by water electrolysis is expected to play a major role in the energy transition, since it can act as a renewable raw material for the chemical industry, a zero emission fuel and a renewable replacement of natural gas in heating applications [1]. Green hydrogen is also a suitable medium for energy storage and can hence provide a system solution to couple variable green electricity supply to inflexible electricity demand.

Yet, water electrolysis based on variable electricity supply also brings new challenges. Using variables loads introduces the need for a wide operating range with a low minimum load in combination with sufficient ramp up rates. This contrasts with the large-scale water electrolysis plants that were operated in the past, which were typically continuously operated based on hydropower [2–4]. Additionally, the variable electricity supply limits the number of operating hours of the electrolysis plant, making the capital costs weigh heavy on the total hydrogen costs. Therefore, there is a strong need for a water electrolysis technology with low capital costs.

Regarding costs, alkaline electrolysis seems to be a well-positioned water electrolysis technology, since it does not require expensive noble materials, which is a limitation of PEM technology, and can be operated at relatively low temperatures hence not requiring high temperature resistant construction materials such as solid oxide technology [5]. However, a major weakness of non-noble metal alkaline technology is that it is operated at relatively low current densities of 0.2–0.6 A cm^{-2} [6,7], making these electrolyzers large and heavy compared to other technologies for similar production rates. This is caused by the "poor" current-voltage curve of alkaline technology, which primarily results from a high ohmic resistance [8]. In old alkaline electrolyzers this high ohmic resistance was almost unavoidable, since only thick asbestos diaphragms were sufficiently stable in the strongly alkaline environment [2]. Yet, with the development of new and thinner diaphragm materials with higher conductivity [9–12], advanced electrode coatings [13–18] and innovative cell concepts [19,20] it should now be possible to develop alkaline electrolysis systems that can operate efficiently at significantly higher current densities.

In the discussion on increased current density it is important to consider that electrolyzer systems are designed for a certain nominal or maximal current density and corresponding cell potential. The unit operations surrounding the electrolyzer, such as the power electronics, the gas-liquid separators and the coolers are designed for operation at this nominal current density and operation at a higher current density is typically not possible (some electrolyzer systems on the market have an "overdrive", but this implies that the surrounding unit operations are overdesigned). The nominal current density is typically selected based on a trade-off between the capital and operational costs of an electrolyzer. A lower nominal current density results in a better efficiency of the plant reducing electricity costs but means that more electrolyzers are needed to make the same amount of hydrogen, resulting in higher capital costs. In practice electrolyzer systems typically have a nominal current density corresponding to an efficiency of 75–80% (based on the higher heating value of hydrogen) at start-of-life, which corresponds to a cell potential of 1.85–1.97 V [7].

The flexibility requirements imposed by the variable electricity supply also have significant implications for the electrolysis technology. Ramp rates are generally sufficiently fast, but the minimum load, which is the lowest load or current density at which an electrolyzer can be safely operated, can be a major limitation. For alkaline electrolyzers this minimum load varies from 10 to 40% [6] and is primarily determined by the volume fraction of hydrogen in oxygen (HTO). Above 4% hydrogen in oxygen the mixture is explosive [21,22] and therefore a maximum of 2% for HTO has been agreed upon in the International Standard on hydrogen production using water electrolysis [23]. This means that at 2% HTO an emergency stop needs to be initiated. Industrial water electrolysis systems are designed to stay significantly below this value to avoid frequent emergency stops. Therefore, an alarm value of 1.6% HTO is typically employed. The HTO content results from hydrogen crossover through the diaphragm and depends on many factors, including diaphragm properties (porosity, tortuosity and thickness), operating pressure and temperature, use of separate or combined electrolyte circuits, and current density [24–28]. At lower current densities, the oxygen production rate is lower compared to the hydrogen gas crossover rate. Therefore, higher values for HTO will be encountered at lower loads. The minimum load of an electrolyzer system is the load were the HTO content reaches 1.6%.

When designing a high current density and flexible alkaline electrolyzer, trade-offs need to be made, since parameters that lead to a lower ohmic resistance generally lead to a higher gas crossover. This is the case for a thinner diaphragm and a temperature increase. When making these trade-offs also other factors such as total plant costs and material durability need to be considered. For example, a lower pressure decreases gas crossover and hence reduces the minimum load, but leads to increased downstream compression costs. Another example is the effect of temperature on the material lifetime and hence durability of the plant.

A key question is what the optimal operating parameters are for advanced alkaline systems. One study into this topic suggests that there is still significant room for optimization of alkaline technology by reducing diaphragm thickness [29]. However, a limitation in that analysis was the limited availability of experimental data to validate the model equations, both with regard to current-voltage curves and gas crossover. A problem is that most experimental studies only report current-voltage curves for one temperature and pressure (mostly atmospheric). The few studies that have systematically looked at temperature and pressure dependence [30–33] have been carried out with relatively poor performing alkaline electrolyzers and as a result do not report any experimental data above 0.4 A cm^{-2}. With regard to hydrogen gas crossover the amount of experimental data was even more limited, but fortunately some recent work has been carried out on the topic [24–27].

In this study we will systematically investigate the optimal operating conditions for an advanced alkaline electrolyzer with regard to temperature, pressure and diaphragm thickness. Goal is to determine operating parameters that enable efficient (80% efficiency corresponding to a cell potential of

1.85 V) operation at high current densities and at the same time have a minimum load that is not higher than 10% of the nominal load. We will carry out this investigation in a temperature range of 60–100 °C, since higher temperatures result in high corrosion rates and an associated need for expensive construction materials. The investigated pressure range is 1–50 bara, since higher pressures would result in the need for thick "rims" of the electrolyzer. Diaphragm thickness is investigated over a range of 100–500 μm, with thinner diaphragms not being investigated for reasons of mechanical strength. We assume constant diaphragm porosity and tortuosity independent of thickness. With regard to electrolyte circulation both the option with separated (no mixing of anolyte and catholyte) and mixed circuits will be investigated. The KOH concentration in this work is not taking as a variable and is set at 30 wt%, which is close to the maximum in conductivity [34]. A higher KOH concentration is regarded as undesirable due to the increase in corrosion rates limiting material selection [35].

For our analysis on the optimal operating conditions we will use both an electrochemical and a gas crossover model. As a basis for the electrochemical model we will use data from an advanced alkaline electrolyzer located at the Brandenburg University of Technology [36,37]. This electrolyzer with a nominal hydrogen production of 20 Nm^3/h consists of 24 cells with an electrode area of 0.436 m^2, has a maximum operating temperature of 75 °C and a maximum pressure of 58 bara. It can be operated at current densities up to 0.72 A cm^{-2}. It has a zero-gap design with perforated nickel electrodes, with an uncoated anode and a cathode coated with Raney nickel. The electrolyte is 28 wt% KOH and Zirfon UTP500 is used as diaphragm. Systematic experiments have been carried out with this electrolyzer over a temperature range of 50–70 °C and a pressure range of 10–55 bara [36]. Our electrochemical model is less complex than some more extended models [32,38–41], but still shows good correspondence with the available experimental data. In this study the model will be used to predict electrolyzer performance over a wider temperature range. Data from another study are used to estimate the dependence of the current-voltage curve on diaphragm thickness [10]. The gas crossover model is made based on best available insights on different hydrogen crossover mechanisms, including diffusive, convective and electrolyte mixing. Parameters in the model are fitted based on available experimental data for Zirfon UTP500 [24–27].

Model description

Current-voltage model

A semi-empirical model has been made for the prediction of the cell potential E_{cell} as a function of current density, temperature and pressure. It considers contributions from the equilibrium cell potential E_{rev}, the combined overpotentials of anode and cathode η_{A+C}, and the ohmic potential drop IR according to equation (1).

$$E_{cell} = E_{rev} + \eta_{A+C} + IR \tag{1}$$

For the calculation of the equilibrium cell potential $E_{rev,T,p}$ equations (2) and (3) as given by LeRoy were employed [42], in which the reversible potential ($E_{rev,T,p}$) depends on the absolute pressure p_0 (in bara), the aqueous vapor pressure of the electrolyte solution p_{H2O} (in bar), the vapor pressure of pure water p^0_{H2O} (in bar) and the reversible potential for standard pressures $E^0_{rev,T}$. The latter can be calculated using equation (3), where the temperature T is in Kelvin. The vapor pressure p_{H2O} for the 30 wt% KOH electrolyte can be found in the literature [43,44]. $\overline{R}$ represents the molar gas constant and F is the Faraday constant.

$$E_{rev} = E^0_{rev} + \frac{\overline{R}T}{2F} ln \frac{\left(p_0 - p_{H_2O}\right)^{1.5}}{\left(p_{H_2O}/p^0_{H_2O}\right)} \tag{2}$$

$$E^0_{rev} = 1.5184 - 1.5421 \cdot 10^{-3} T + 9.523 \cdot 10^{-5} T ln T + 9.84 \cdot 10^{-8} T^2 \tag{3}$$

Data from the work of Fischer [36] (data shown in Supplementary Information) was analyzed to determine values for the combined overpotentials and ohmic resistance that a representative of a state-of-the-art alkaline electrolyzer. The current-voltage relationships were first individually fitted according to the procedure described in Ref. [8]. In this fitting process the Tafel slope, the exchange current density and the ohmic resistance were used as fitting parameters. The combined overpotentials depend on the Tafel slope b, the current density I and the exchange current density I_0 according to equation (4). In this equation b is defined $b = a + c$ in which a is the Tafel slope of the anode and c is the Tafel slope of the cathode. I_0 is a non-linear average of the anodic and cathodic exchange current densities, according to $I_0 = I_{0,a}^{a/b} I_{0,c}^{c/b}$ [8]. The fitted values for the different operating pressures and temperatures can be found in the Supplementary Information.

$$\eta_{A+C} = b \log_{10} \frac{I}{I_0} \tag{4}$$

As a next step the fitted values were analyzed as a function of temperature. The Tafel slopes b did show a linear increase with temperature (see Supplementary information), as one would expect based on equation (5), which results from the Butler-Vollmer equation and which includes a factor 2 because b represents the combined Tafel slopes of the anode and cathode. α_{app} is the apparent charge transfer coefficient, a non-linear average of the anodic and cathodic charge transfer coefficients, according to $\alpha_{app} = \frac{2\alpha_a \alpha_c}{\alpha_a + \alpha_c}$. The measured temperature dependence corresponds to an apparent charge transfer coefficient of 1.20. This value exceeds the typical value of 0.5, which suggests that the first electron transfer is neither the rate-limiting step for hydrogen evolution on Raney-Ni electrodes nor for oxygen evolution on nickel electrodes. This is in line with the observation that the fitted b values are ~110 mV, implying that individual Tafel slopes of anode and cathode must be well below 100 mV, which agrees with previous work [45,46].

$$b = \frac{2\overline{R}T \ln 10}{\alpha_{app} F} \tag{5}$$

The logarithm of the fitted exchange current densities I_0 showed a linear dependence with the reverse of the temperature (see Supplementary information), in line with an Arrhenius-type dependence, as given by equation (6), in which k_0 is a prefactor (a non-linear average of the prefactors for anodic and cathodic exchange current densities: $k_0 = k_{0,a}^{a/b} k_{0,c}^{c/b}$) and ΔG_{act} is an average of the activation energies of the oxygen and hydrogen evolution according to $\Delta G_{act} = (a\Delta G_{act,a} + c\Delta G_{act,c})/b$. From the fitting a value of 29.5 A cm^{-2} results for k_0 and 32.4 kJ mol^{-1} for ΔG_{act}. The value of ΔG_{act} is relatively low compared to values reported in literature, which range from 18 to 104 kJ mol^{-1} [38,46]. Combining equations (4)–(6) results in equation (7) for the dependence of the combined overpotentials on the temperature and the current density.

$$I_0 = k_0 e^{\frac{-\Delta G_{act}}{\overline{R}T}} \tag{6}$$

$$\eta_{A+C} = \frac{2\overline{R}T \ln 10}{\alpha_{app} F}\left(\log_{10}\frac{I}{k_0} + \frac{\Delta G_{act}}{\overline{R}T ln 10}\right) \tag{7}$$

The fitted ohmic resistances R showed a strong dependence on temperature, comparable to the temperature dependence of the resistance of the 28 wt% electrolyte (see Supplementary Information). The resistance R as a function of temperature can therefore be predicted reasonably well by equation (8), in which $R_{60°C}$ is the fitted resistance at 60 °C and $\kappa_{60°C}$ is the solution conductivity at 60 °C. The solution conductivity κ can be calculated for different KOH molarities M with equation (9) [34]. To be able to predict the effect of diaphragm thickness d (in mm) a correction factor is included in equation (8), which is based on two studies in which Zirfon of two thicknesses were studied [10,25]. It should be noted that the resistance is not directly proportional to the thickness of the diaphragm. This can be explained by the observation that the ohmic resistance significantly exceeds the pure diaphragm resistance [8], which suggests that the diaphragm resistance is not the only contributor to the ohmic resistance in a zero-gap configuration. For example, the presence of bubbles is believed to be responsible for a significant extra resistance outside the diaphragm [47]. Nevertheless, there is still a high uncertainty in the dependence of resistance on diaphragm thickness, because it is currently based on only two diaphragm thicknesses. Moreover, the comparison of the two diaphragms could potentially be affected by a difference in tortuosity.

$$R = R_{60°C}\frac{\kappa}{\kappa_{60°C}}(0.26 + 1.48d) \tag{8}$$

$$\kappa = -2.04M - 2.8\cdot10^{-3}M^2 + 5.33\cdot10^{-3}MT + 207\frac{M}{T} + 1.04\cdot10^{-3}M^3 - 3\cdot10^{-7}M^2T^2 \tag{9}$$

Gas crossover model

The hydrogen in oxygen (HTO) can be calculated from the flux of hydrogen to the anolyte Φ_{H2} and the oxygen production n_{O2} according to equation (10). The hydrogen flux potentially consists of three contributors, namely $\Phi_{H_2,diff}$, which is hydrogen crossover resulting from hydrogen diffusion through the diaphragm, $\Phi_{H_2,conv}$, which is hydrogen crossover as a result of convective flow of electrolyte with dissolved hydrogen through the diaphragm, and $\Phi_{H_2,mix}$, which is hydrogen transported into the anolyte compartment by hydrogen dissolved in the incoming electrolyte stream, according to equation (11).

$$HTO = \frac{\Phi_{H_2}}{n_{O_2} + \Phi_{H_2}} = \frac{\Phi_{H_2}}{\frac{1}{4F} + \Phi_{H_2}} \tag{10}$$

$$\Phi_{H_2} = \Phi_{H_2,diff} + \Phi_{H_2,conv} + \Phi_{H_2,mix} \tag{11}$$

The convective movement of solution through the diaphragm can arise due to different phenomena. Most importantly, convection can be induced if a pressure drop over the diaphragm exists, resulting in electrolyte flow in a particular direction that either enhances or suppresses hydrogen crossover. This convective hydrogen flux depends on the diaphragm permeability K, the dynamic viscosity η, the hydrogen solubility S_{H2}, the partial hydrogen pressure at the membrane interface $p_{H2,m.}$ and most importantly the differential pressure difference between catholyte and anolyte Δp according to equation (12). The permeability of the diaphragm K strongly depends on pore-size and to less extent on other separator characteristics as porosity and tortuosity. For the Zirfon separator with a mean pore size of 150 nm, K is estimated to be $7.5\cdot10^{-16}$ m^{-2} [25]. For the Zirfon separator it has been suggested that at differential pressures above 0.01 bar the convective flux becomes larger than the diffusive flux [48]. For this reason, good pressure control in alkaline systems is of critical importance. This is normally achieved by connecting the liquid sides of the anolyte and catholyte gas-liquid separators and minimizing the difference in liquid level by pressure control valves. As a result, the convective hydrogen transport seems to play a limited role in laboratory scale alkaline electrolyzers. This is also suggested by studies in which Zirfon is compared to diaphragms and membranes with significantly smaller pores [25,27]. With equal pressures on both sides these studies show comparable gas crossover. In contrast, with the application of a differential pressure of 0.3 bar the crossover through the Zirfon becomes much higher [27] suggesting that only then the convective flux start to play an important role (this is explained more in-depth in the Supplementary Information). Nevertheless, it is less clear if convective hydrogen transport can also be neglected in industrial scale electrolyzers, where larger cell areas can potentially result in larger local Δp differences.

$$\Phi_{H_2,conv} = \frac{KS_{H_2}p_{H_2}\Delta p}{\eta d} \tag{12}$$

Electro-osmotic drag or electro-osmotic flow can potentially also contribute to convective hydrogen transport through the diaphragm. Both phenomena arise due to movement of ions in the presence of an electric field, which can drag electro-neutral solvent and dissolved gases along them. However, they are not believed to have a significant contribution in alkaline electrolysis [24] (this is further explained in the Supplementary Information).

The hydrogen transport $\Phi_{H_2,mix}$ resulting from hydrogen dissolved in the incoming electrolyte stream is only relevant for systems where anolyte and catholyte streams are mixed

after the gas-liquid separation, known as combined circuits. In case of separate anolyte and catholyte streams this $\Phi_{H_2,mix}$ can be neglected. In the former case, part of the electrolyte leaving the cathodic side, which is saturated with hydrogen, enters the anodic compartment. In this case the hydrogen transport depends on the anolyte and catholyte flow rates F_{ano} and F_{cato} according to equation (13). For industrial scale electrolysis systems these electrolyte flow rates are typically equal ($F_{ano} = F_{cato}$) and are primarily determined by the allowable temperature difference over the electrolyzer according to equation (14), as the electrolyte flow is the main method for cooling the electrolyzer. In this equation A is the electrode area, E_{tn} is the thermoneutral cell potential, E_{cell}^{eol} is the cell potential at end of life (when most heat is generated, in this work 2.0 V is assumed), C_p is the heat capacity of the electrolyte (3.07 J g^{-1} K^{-1} for 30 wt% KOH electrolyte at 80 °C [49]), ρ is the electrolyte density (1.255 g cm^{-3} at 80 °C [50]) and ΔT is the maximum allowable temperature differences over the cell, which is typically around 15 °C [13]. In this case the thermoneutral cell potential E_{tn} includes both the enthalpic voltage and the effect of the evaporation of water according to equation (15) [51], in which $\Delta H_{vap,\,T}$ is the heat of evaporation of water at the operating temperature (equation (16)). It does not include the heating of the feedwater (since this is added outside the electrolyzer) and any heat losses through radiation and convection.

$$\Phi_{H_2,mix} = S_{H_2} p_{H_2} \left(\frac{F_{ano}}{F_{cat} + F_{ano}}\right) \cdot F_{ano} \tag{13}$$

$$F_{ano} + F_{cato} = \frac{IA\left(E_{cell}^{eol} - E_{tn}\right)}{C_p \Delta T \rho} \tag{14}$$

$$E_{tn} = 1.485 - 1.49 \cdot 10^{-4}(T - 273) - 9.84 \cdot 10^{-8}(T - 273)^2 + 1.5 \cdot \frac{p_{H2O}}{(p_0 - p_{H2O})} \cdot \frac{\Delta H_{vap,\,T}}{2F} \tag{15}$$

$$\Delta H_{vap,\,T} = 42.960 + 40.762 \cdot T - 0.06682 \cdot T^2 \tag{16}$$

In systems with separated electrolyte circuits and good differential pressure control, the diffusive flux is the main driver for crossover through the diaphragm. This diffusive flux can be calculated using equation (17). In this equation $D_{H_2,eff}$ is the effective diffusion coefficient of hydrogen through the separator. S_{H_2} is the solubility of hydrogen in the electrolyte, for which we use a value of 0.095 mol m^{-3} bar^{-1} in 30 wt% KOH [52,53]. The solubility shows limited temperature dependence and is therefore taken as temperature independent in our model (See Supplementary information). $p_{H_2,m}$ is the hydrogen pressure at the catholyte diaphragm interface, including local supersaturation. In this equation the hydrogen pressure at the anode is assumed to small and is therefore not taken into account.

$$\Phi_{H_2,diff} = \frac{D_{H_2,\,eff} S_{H_2} p_{H_2,m}}{d} \tag{17}$$

For a porous diaphragm the effective diffusion coefficient in the diaphragm depends on the diffusion coefficient in the free electrolyte D_{H_2}, the diaphragm porosity ε and the diaphragm tortuosity factor τ^2 (not to be confused with the tortuosity [54]) according to equation (18). Although the porosity for the diaphragm has been measured to be 55% [25], it is not possible to directly measure the tortuosity factor. Therefore, we use the MacMullin number N_m, which is equal to the tortuosity factor divided by the porosity [55]. Normally the MacMullin number is used in relation to resistance, where it gives the ratio between the resistivity of a porous medium and the resistivity of the pure electrolyte. In a similar way it can be used for diffusive transport in a porous medium. A value for the MacMullin number of 3.2 has been suggested based for Zirfon UTP500 on available experimental data [8]. The diffusion coefficient D_{H_2} has been reported to show an Arrhenius type dependence as given in equation (19). For a 30 wt% KOH electrolyte the prefactor A in this equation is $4.7 \cdot 10^{-4}$ m^2 s^{-1} and the activation energy E_a is 19.8 kJ mol^{-1} [56].

$$D_{H_2,\,eff} = D_{H_2} \cdot \frac{\varepsilon}{\tau^2} = \frac{D_{H_2}}{N_m} \tag{18}$$

$$D_{H_2} = A e^{\frac{-E_a}{RT}} \tag{19}$$

The main challenge in estimating the diffusive hydrogen flux lies in the uncertainty concerning local supersaturation at the electrode-diaphragm interface in a zero-gap configuration. It is well-known that there can be significant local supersaturation in the concentration boundary layer of gas-evolving electrodes, more than hundred times the solubility [57–59]. However, it is difficult to say how this translates to a supersaturation at the electrode-diaphragm interface, since the concentration boundary layer is relatively thin (order of μms [60]) and a zero-gap configurations is normally not perfect "zero-gap", since only a small part of the electrode material pushes directly against the membrane. For PEM electrolyzers large supersaturations that strongly depend on current density have been reported (8–33 bar A^{-1} cm^{-1}) [61], but for zero-gap alkaline electrolyzers no correlations are available. A more in-depth discussion on local supersaturation can be found in the Supplementary Information.

In this work, available experimental data on hydrogen crossover through a Zirfon separator have been used to determine a relation between hydrogen concentration at the diaphragm-electrode interface and the operating conditions. It is assumed that the hydrogen is only supersaturated at the electrodes. As some experimental studies have used larger separator than electrode areas, diffusion through the separator where no electrode is attached to the surface, is modeled using equilibrium concentration $p_{H_2,eq}$. In total, 43 HTO data points from four different studies were used for fitting (listed in Supplementary Information), including data from mixed and separate electrolyte loops. The assumption has been made that hydrogen crossover by convection can be neglected. The hydrogen pressure at the catholyte diaphragm interface $p_{H_2,m}$ is fitted as a function of the square roots of the current density and the absolute pressure p_0 according to equation (20). The reason for taking the square roots of the current density and pressure is that the supersaturation not only depends on the amount of hydrogen generation (directly proportional to the current density), but also on the available

bubble area and mass transfer rates (which increase with current density and decrease with pressure). This is discussed in more depth in the Supplementary Information. The square root dependencies also seem to fit well with the experimental data. Based on a fit of all experimental data with a total R^2 of 0.994 the value for the constant f was determined to be 25.80 for 30 wt% KOH (More information on the fitting procedure can be found in the Supplementary Information).

$$p_{H_2,m} = p_0 - p_{H_2O} + fI^{0.5}p_0^{0.5} \quad (20)$$

Table 1 summarizes the parameters that can be used to describe current-voltage model consisting of equations (1), (2), (7) and (8) and the gas crossover model consisting of equations (10) and (13)–(15).

Results and discussion

Comparison of the models to experimental data

Fig. 1 compares the cell potential predicted by the current-voltage model to the experimental data for different temperatures and pressures [36]. The temperature dependence is described well by the model with higher temperatures leading to lower cell potentials. This is primarily driven by a lower ohmic resistance at increased temperature, but also the overpotentials are slightly lower at increased temperature. For the pressure dependence the model also gives a reasonable prediction, although it seems to slightly overpredict pressure dependence. Pressure dependence is now only included in the model in the equilibrium potential (equation (2)), but not in the description of the overpotentials and the ohmic resistance. A lower pressure is expected to lead to increased gas volume in the electrolyte and an increased electrode surface coverage [58], both increasing the cell potential. Yet, these effects are relatively small and still not well understood and have therefore not been included in the model to reduce its complexity.

Fig. 2 compares HTO content predicted by the model to a number experimental data generated by Trinke et al. [24]. Comparison to all other experimental data points is given in the Supplementary Information, which shows that the model can accurately predict the experimental data. Hence it is possible to describe the experimental results with only the diffusive flux and is therefore another indication that with separated circuits the gas crossover is primarily driven by the diffusive flux through the diaphragm and not by pressure or electro-osmotic driven convection. This is also confirmed by the fact that the model can reasonably predict the OTH content (see Supplementary Information). However, we should note that our model is unable to predict available HTO and OTH data for a thinner diaphragm [25], with our model predicting significantly higher gas crossover than observed. We do not yet understand why this is the case. It has been suggested that the thinner diaphragm has a higher tortuosity suppressing the gas crossover [25], but in our view there is no reason why the thinner diaphragm should have a much higher tortuosity given that it has the same porosity as the thick diaphragm and is produced in a comparable way. Moreover, a higher tortuosity would also affect diaphragm conductivity, which is not observed [62].

Table 1 – Input values for the current-voltage model and the gas crossover model.

α_{app}	1.20
k_0	29.5 A cm^{-2}
ΔG_{act}	32.4 kJ mol^{-1}
$R_{60°C}$	0.446 Ω cm^{-2}
N_m	3.2
A	$4.7 \cdot 10^{-4}$ m^2 s^{-1}
E_a	19.8 kJ mol^{-1}
S_{H2}	0.095 mol m^{-3} bar^{-1}
f	25.80
ΔT	15 K
E_{cell}^{eol}	2.0 V

Model extrapolation to find optimal operating conditions

In this section we use our models to explore how electrolyzer performance is likely to change with varying temperature, pressure and diaphragm thickness. We do this in a temperature range of 60–100 °C, a pressure range of 1–50 bara and a diaphragm thickness of 0.1–0.5 mm. We realize that especially regarding temperature this is beyond the range in which the model has been validated, but we feel that the correlations we use are sufficiently robust to give a reasonable prediction up to 100 °C.

Fig. 3 shows the predicted current-voltage curves for different temperatures and diaphragm thicknesses at an operational pressure of 10 bara. It shows that both a higher temperature and a smaller diaphragm thickness improve the current-voltage curve and therefore enable a higher nominal current density. Based on the starting point that the nominal current density corresponds to a cell potential of 1.85 V, the nominal current density at 60 °C with a 0.5 mm diaphragm is 0.5 A cm^{-2}. At 100 °C with a 0.1 mm diaphragm it is more than three times as high at 1.7 A cm^{-2}. This much higher current density is primarily enabled by the lower ohmic resistance resulting from the higher temperature and reduced diaphragm thickness, but also from the reduced overpotentials at increased temperature. The advantages of a temperature increase have long been recognized in the field of alkaline electrolysis and have resulted in significant efforts to develop high temperature alkaline electrolyzers in the past [63–65]. Yet, it should be remarked that this has not proven to be easy due to material limitations. Therefore, we have chosen not to explore temperatures above 100 °C.

Fig. 4 shows the HTO content as a function of current density for temperatures of 60 °C, 80 °C and 100 °C with a 0.5 mm and a 0.1 mm diaphragm at a pressure of 10 bara. It shows that both decreased diaphragm thickness and increased temperature lead to increased HTO content. For 60 °C and a 0.5 mm diaphragm the HTO content remains low even for low current densities, which means that the minimum load is not limited by gas purity. On the other hand, for 100 °C and a 0.1 mm diaphragm the HTO content exceeds 1.6% below 0.4 A cm^{-2}, which means that the minimum current density is 0.4 A cm^{-2}. Considering that the nominal current density for these conditions is 1.7 A cm^{-2} (see previous paragraph), this implies that the minimum load is ~25%,

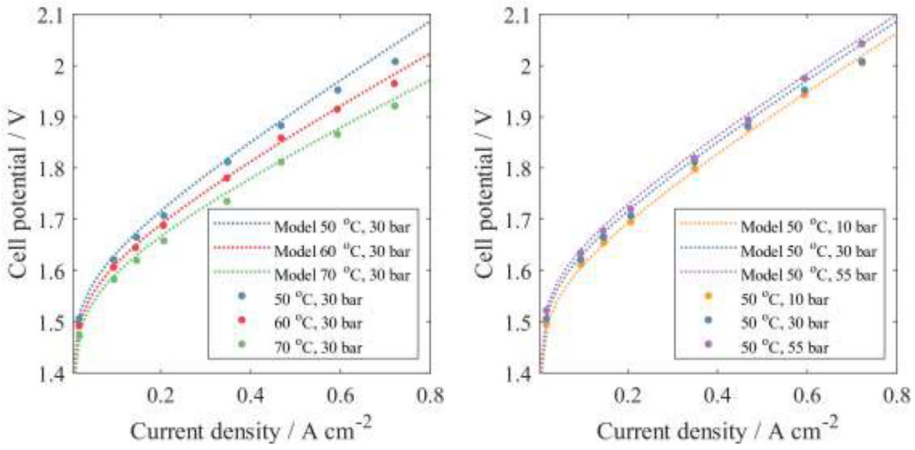

Fig. 1 – Cell potential as a function of current density predicted by the current-voltage model compared to experimental data of a zero-gap alkaline electrolyzer [36] for different temperatures (left) and pressures (right). 28 wt% KOH and Zirfon UTP500 diaphragm.

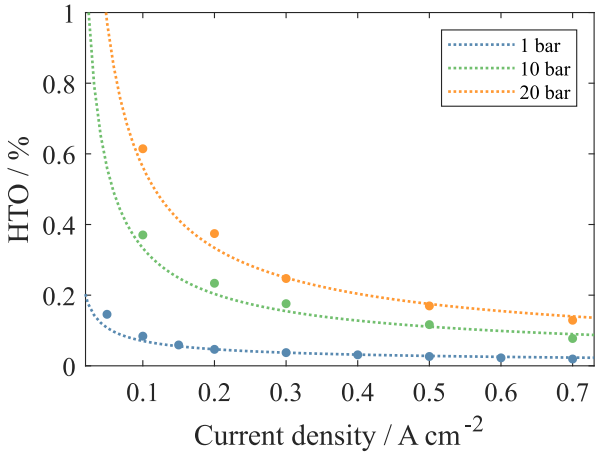

Fig. 2 – HTO content predicted by the gas crossover model compared to experimental data of Trinke et al. [24]. Conditions: 1 bara, 60 °C, Zirfon UTP500, 32 wt% KOH, electrode area = 100 cm^2, diaphragm area = 227 cm^2, separated electrolyte circuits.

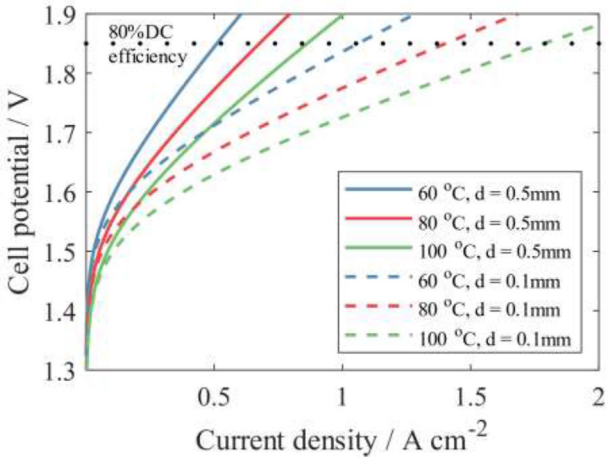

Fig. 3 – Predicted current-voltages curves for temperatures of 60 °C, 80 °C and 100 °C with a 0.5 mm and a 0.1 mm diaphragm. Pressure = 10 bara, 30 wt% KOH.

significantly higher than our target value of 10%. Hence, the combination of 100 °C, 10 bara and a 0.1 mm diaphragm is not suitable for a flexible alkaline electrolyzer.

As discussed previously, the influence of pressure on the current-voltage curve is limited. In contrast, pressure does have a large influence on the gas crossover. This can be seen in Fig. 5, which shows the HTO content for a system operating at 100 °C with a 0.1 mm Zirfon diaphragm for different pressures. At atmospheric pressure the HTO content remains below 1.6% even at very low current densities. In contrast, at 20 bara the HTO content is already 1.6% at 0.6 A cm^2 for separated circuits. Considering the nominal current density of 1.7 A cm^{-2}, this implies that for an atmospheric electrolyzer it is easy to meet the 10% minimum load requirement, but that this requirement cannot be met for operation at 10 or 20 bara. Actually, the maximum allowable operating pressure with separated circuits to enable a minimum load of 10% is 5 bara with a HTO content of 1.6% at 0.17 A cm^{-2}.

Fig. 5 also shows the effect of the use of a mixed electrolyte system, in which dissolved hydrogen coming from the cathode compartment enters the anode compartment due to the mixing of the electrolytes after the gas-liquid separators. As expected, this electrolyte mixing leads to an increased HTO content. The effect becomes more pronounced with higher pressure, due to the increase in the concentration of dissolved hydrogen with increasing pressure. Nevertheless, even for high pressures this mixing contribution to the HTO content remains significantly lower than the diffusive transport. This contrasts with the conclusions from others [24,26,28], which argue that electrolyte mixing is the dominant factor in HTO content even at atmospheric pressure. The reason for this apparent difference are the much higher flow rates that are used in laboratory electrolyzers compared to industrial electrolyzers. This is illustrated by the fact that anolyte flow rates of ~30 l/h were used in the laboratory cells [24,26], whereas to

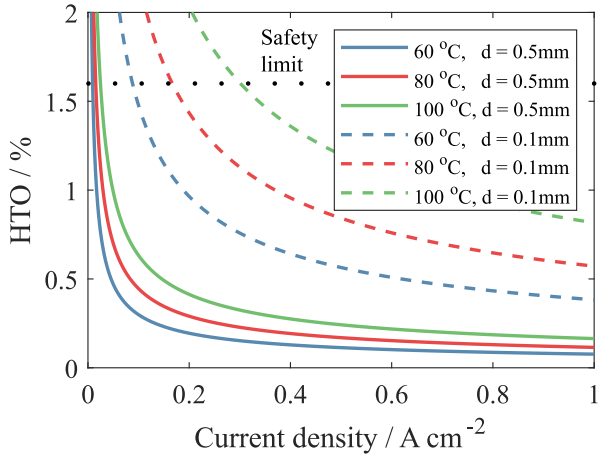

Fig. 4 – Predicted HTO content as a function of current density for temperatures of 60 °C, 80 °C and 100 °C with a 0.5 mm and a 0.1 mm Zirfon diaphragm. Pressure = 10 bara, 30 wt% KOH. Separated cycles.

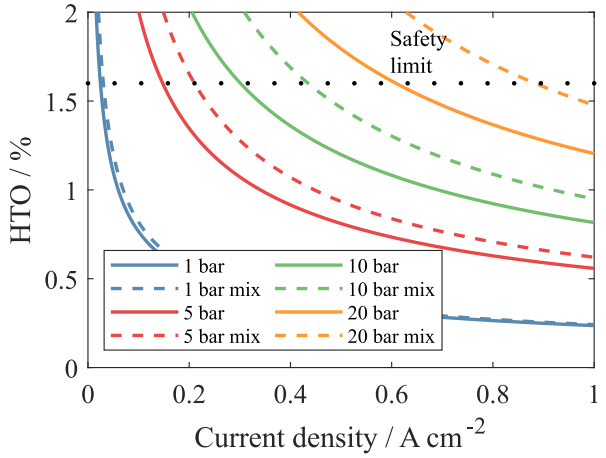

Fig. 5 – Predicted HTO content as a function of current density for pressures of 1, 5, 10 and 20 bara. Operational temperature is 100 °C, 0.1 mm Zirfon diaphragm, 30 wt% KOH. Mixed circuits data are modeled with an anolyte flow of 2.84 l/h and a catholyte flow of 2.84 l/h for a 100 cm^2 cell, based on a nominal current density of 1.7 A cm^{-2} and an E_{cell}^{eol} of 2.0 V.

keep the temperature difference below 15 °C it can be calculated with equation (15) that a flow rate of only ~1 l/h is required (for a 100 cm^2 electrode at 0.5 Acm^{-2}). It is important to note that the contribution of electrolyte mixing to HTO content is independent of diaphragm thickness and temperature. This makes that with lower operating temperatures and higher diaphragm thicknesses the contribution of electrolyte mixing to the HTO content becomes relatively more important as diffusive transport decreases.

To find the optimal operating parameters for an alkaline electrolyzer the contour plots in Figs. 6 and 7 are used. Fig. 6 shows what nominal current density can be achieved for different temperatures and diaphragm thicknesses. This

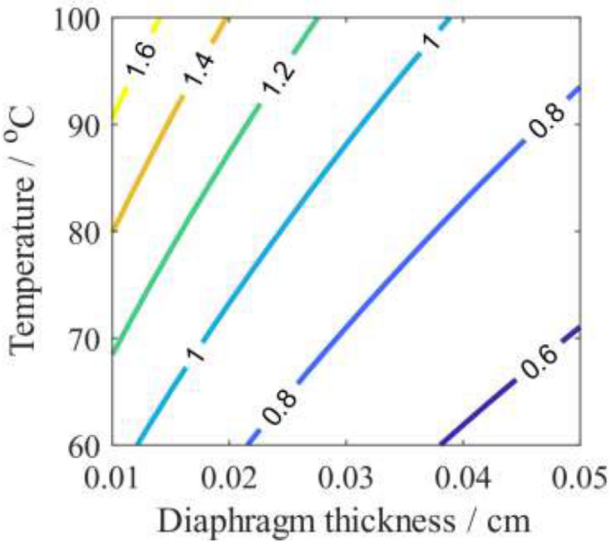

Fig. 6 – Contour plot of the nominal current density as a function of temperature and diaphragm thickness for a zero-gap alkaline electrolyzer with an activated Raney-Ni cathode. Pressure = 10 bara, 30 wt% KOH. At the nominal current density the cell potential is 1.85 V.

graph is based on a pressure of 10 bara, but the dependence of the nominal current density on the pressure is limited and therefore graphs at other pressures are comparable (shown in Supplementary information). The highest achievable current density is 1.8 A cm^{-2} at a temperature of 100 °C and a diaphragm thickness of 0.1 mm.

Fig. 7 shows the maximum allowable pressure to enable a minimum load corresponding to 10% of the nominal current densities given in Fig. 6. These values are hence based on a nominal current density at 10 bar, but the values are comparable when nominal current densities at other pressures are used (see Supplementary information). Fig. 7 shows data for both separated (left) and mixed systems (middle and right). The figures for the mixed system are based on either a constant (middle) or variable electrolyte flow rate (right). The constant flow rate corresponds to a temperature difference over the electrolyzer of 15 °C at end-of-life. For the variable flow rate this flow rate is adjusted based on the operating current density. The latter enables a significantly higher operating pressure, close to the value of the separated system.

In the discussion on the optimal operating parameters, we also consider that higher pressures can be regarded as more attractive, since they reduce compression requirements. They also reduce the gas hold-up in electrolyzers [66] enabling increased ramping rates, since ramp rates are limited by the changes in gas hold-up. On the other hand, higher pressures do lead to higher stack costs and increase safety risks. Another consideration is the material choice for the electrolyzer and the surrounding unit operations. Up to approximately 80 °C relatively cheap carbon steel can be used as construction material if stress relief heat treatment is applied, but at higher temperatures it is needed to use more expensive nickel alloys or even pure nickel to avoid stress corrosion cracking [35,67].

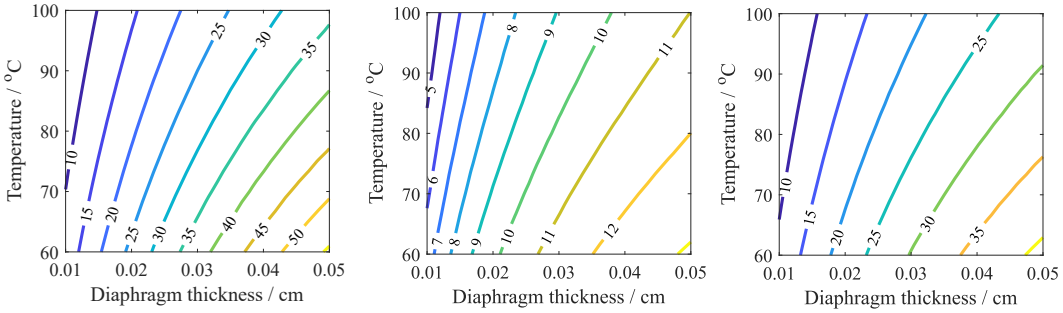

Fig. 7 – Contour plots of the maximum allowable pressure to enable a minimum load of 10% based on the nominal current density for 10 bar as plotted in Fig. 6, with separated circuits (left) and combined circuits (middle and right). For the mixed circuits system, either a constant flow rate (middle) or a variable flow rate (right) is used. This flow corresponds to a temperature difference over the electrolyzer of 15 °C at end-of-life. For the variable flow rate the flow rate is 10% of the flow rate at nominal load.

Based on the above considerations there are three potentially attractive systems. The first is a low-temperature (60–80 °C) high-pressure system with a thick diaphragm and separated circuits. Such a system can be operated with a nominal current density of up to 0.7 A cm^{-2} and pressures in the range of 30–50 bara. In this way it is similar to the electrolyzer of the Brandenburg University of Technology that was used as a basis for the current-voltage model in this work. Strengths of this system are the high operating pressure, reducing compression needs, and the relatively cheap construction materials. Weaknesses are the low current density, higher stack costs and the use of separated circuits, increasing the complexity of the plant. Overall, these operating conditions seem most suitable for relatively small-scale electrolyzer systems, where the capital costs of the compression are a key cost driver.

The second is a low-temperature (60–80 °C) and low-pressure system with a thin diaphragm and combined circuits. Such a system can be operated with a nominal current density of up to 1.4 A cm^{-2} and a pressure up to 7.5 bara. Strengths of this system are the high current density, the relatively cheap construction materials and the ability to use mixed circuits. Weakness is the relatively low pressure, increasing compression costs. Overall, these operating conditions seem suitable for the deployment of large-scale electrolyzer systems, where the capital costs of the required compression steps can be kept small due to the good economies of scale of compression. Operation at this pressure still avoids the first compression steps, which are the most capital intensive. Therefore, these operating conditions are significantly more attractive than operating at atmospheric pressure.

The third system is a high-temperature (80–100 °C) low-pressure system with a thin diaphragm and combined circuits. Such as system can be operated with a nominal current density of up to 1.8 A cm^{-2} and a pressure up to 5 bara. This system is comparable to the previously discussed low temperature system with the difference that the nominal current density is slightly higher and that more expensive construction materials will need to be used. Question is whether the higher nominal current density is enough to compensate the increased material costs. Nevertheless, there can be additional reasons to choose this high-performance system: the higher operating temperatures make it easier to valorize the generated waste heat and the high current density is attractive in places where plant footprint is a limitation. This makes this system potentially attractive for large-scale systems where waste heat and footprint are important.

Our analysis also shows that certain operating parameters are unattractive. These include high-pressure systems (>10 bara) with thin diaphragms. These systems can potentially achieve a high nominal current density, but are limited by their high minimum load, making them less suitable for operation with variable renewable electricity supply. At the same time also high-temperature systems with thick diaphragms seem unattractive, since they require the use of expensive construction materials without being able to reach high nominal current densities.

We should remark that there are still significant uncertainties in the modeling. Most problematic is the limited availability of experimental data for thinner diaphragms, which causes a significant uncertainty regarding the dependence of the ohmic cell resistance and gas crossover on the diaphragm thickness. Other uncertainties include the extent of local supersaturation, and the role of convective transport in gas crossover. Therefore, there is a clear need for more experimental data to optimize these models. Future optimization could still significantly affect achievable nominal current densities and allowable operating pressures. Nevertheless, we believe that our more general conclusions on the optimal operating parameters will still hold.

Conclusion

In this work we have investigated the influence of temperature, pressure and diaphragm thickness on the performance of alkaline electrolyzers. Whereas traditional alkaline electrolyzers with non-noble metal catalysts are operated at low current densities (0.2–0.4 A cm^{-2}), our current-voltage model shows that it should be possible to operate advanced alkaline electrolyzers above 1 A cm^{-2} by applying a zero-gap design, reducing diaphragm thickness and increasing temperature.

However, these operating parameters also enhance gas crossover and can lead to high HTO levels at low load, which is problematic for intermittent electrolysis systems based on solar and wind energy. Our gas crossover model shows that HTO levels at a minimum load of 10% can be kept at an acceptable level by keeping the operating pressure below 8 bara, also with mixed electrolyte systems. Given that the relative costs of compression decrease with increasing system size, operating at these pressure levels seems most attractive for future large-scale electrolysis plants.

Declaration of competing interest

The authors declare that they have no known competing financial interests or personal relationships that could have appeared to influence the work reported in this paper.

Appendix A. Supplementary data

Supplementary data to this article can be found online at https://doi.org/10.1016/j.ijhydene.2022.08.075.

REFERENCES

[1] International Energy Agency. The future of hydrogen. 2019. https://doi.org/10.1787/1e0514c4-en.

[2] Tilak BV, Lu PWT, Colman JE, Srinivasan S. Electrolytic production of hydrogen. In: Bockris JO, editor. Compr. Treatise electrochem. New York: Plenum Press; 1981. p. 1–104.

[3] Smolinka T, Bergmann H, Garche J, Kusnezoff M. The history of water electrolysis from its beginnings to the present. Elsevier B.V.; 2022. https://doi.org/10.1016/b978-0-12-819424-9.00010-0.

[4] Sandstede G, Wurster R. Water electrolysis and solar hydrogen demonstration projects. In: White RE, editor. Mod. Asp. electrochem. Number 27. Plenum Press; 1995. p. 411–514.

[5] IRENA. Green hydrogen cost reduction: scaling up electrolysers to meet the 1.5^{0}C climate goal. 2020.

[6] Schmidt O, Gambhir A, Staffell I, Hawkes A, Nelson J, Few S. Future cost and performance of water electrolysis: an expert elicitation study. Int J Hydrogen Energy 2017;42:30470–92. https://doi.org/10.1016/j.ijhydene.2017.10.045.

[7] Europe Hydrogen. Strategic research and innovation agenda 2021-2027. 2022.

[8] de Groot MT, Vreman AW. Ohmic resistance in zero gap alkaline electrolysis with a Zirfon diaphragm. Electrochim Acta 2021;369. https://doi.org/10.1016/j.electacta.2020.137684.

[9] Vermeiren P, Adriansens W, Leysen R. Zirfon®: a new separator for Ni-H2 batteries and alkaline fuel cells. Int J Hydrogen Energy 1996;21:679–84. https://doi.org/10.1016/0360-3199(95)00132-8.

[10] Loos S. Active anodes for alkaline water electrolysis. Adv. alkaline electrolysis. 3rd Ind. Work.; 2020.

[11] Lee JW, Lee JH, Lee CS, Cho HS, Kim MJ, Kim SK, et al. Cellulose nanocrystals–blended zirconia/polysulfone composite separator for alkaline electrolyzer at low electrolyte contents. Chem Eng J 2022;428:131149. https://doi.org/10.1016/j.cej.2021.131149.

[12] Kim S, Han JH, Yuk J, Kim S, Song Y, So S, et al. Highly selective porous separator with thin skin layer for alkaline water electrolysis. J Power Sources 2022;524:231059. https://doi.org/10.1016/j.jpowsour.2022.231059.

[13] De Nora. De nora electrodic package for alkaline water electrolysis. 2020.

[14] Ďurovič M, Hnát J, Bouzek K. Electrocatalysts for the hydrogen evolution reaction in alkaline and neutral media. A comparative review. J Power Sources 2021;493. https://doi.org/10.1016/j.jpowsour.2021.229708.

[15] Razmjooei F, Liu T, Azevedo DA, Hadjixenophontos E, Reissner R, Schiller G, et al. Improving plasma sprayed Raney-type nickel–molybdenum electrodes towards high-performance hydrogen evolution in alkaline medium. Sci Rep 2020;10. https://doi.org/10.1038/s41598-020-67954-y.

[16] Chung DY, Lopes PP, Farinazzo Bergamo Dias Martins P, He H, Kawaguchi T, Zapol P, et al. Dynamic stability of active sites in hydr(oxy)oxides for the oxygen evolution reaction. Nat Energy 2020;5:222–30. https://doi.org/10.1038/s41560-020-0576-y.

[17] Bernäcker CI, Rauscher T, Büttner T, Kieback B, Röntzsch L. A powder metallurgy route to produce raney-nickel electrodes for alkaline water electrolysis. J Electrochem Soc 2019;166:F357–63. https://doi.org/10.1149/2.0851904jes.

[18] Burke MS, Enman LJ, Batchellor AS, Zou S, Boettcher SW. Oxygen evolution reaction electrocatalysis on transition metal oxides and (Oxy)hydroxides: activity trends and design principles. Chem Mater 2015;27:7549–58. https://doi.org/10.1021/acs.chemmater.5b03148.

[19] Swiegers GF, Terrett R, Tsekouras G, Tsuzuki T, Pace R, Stranger R. The prospects of developing a highly energy-efficient water electrolyser by eliminating or mitigating bubble effects. Sustain Energy Fuels 2021;5:1280–310. https://doi.org/10.1039/D0SE01886D.

[20] Lee HI, Cho HS, Kim MJ, Lee JH, Lee CS, Lee S, et al. The structural effect of electrode mesh on hydrogen evolution reaction performance for alkaline water electrolysis. Front Chem 2021;9:1–10. https://doi.org/10.3389/fchem.2021.787787.

[21] Schroeder V, Holtappels K. Explosion characteristics of hydrogen-air and hydrogen-oxygen mixtures at elevated pressures. Int Conf Hydrog Saf 2005. Paper No. 120001.

[22] Janssen H, Bringmann JC, Emonts B, Schroeder V. Safety-related studies on hydrogen production in high-pressure electrolysers. Int J Hydrogen Energy 2004;29:759–70. https://doi.org/10.1016/j.ijhydene.2003.08.014.

[23] ISO22734. Hydrogen generators using water electrolysis-Industrial, commercial, and residential applications. 2019.

[24] Trinke P, Haug P, Brauns J, Bensmann B, Hanke-Rauschenbach R, Turek T. Hydrogen crossover in PEM and alkaline water electrolysis: mechanisms, direct comparison and mitigation strategies. J Electrochem Soc 2018;165:F502–13. https://doi.org/10.1149/2.0541807jes.

[25] Brauns J, Schönebeck J, Kraglund MR, Aili D, Hnát J, Žitka J, et al. Evaluation of diaphragms and membranes as separators for alkaline water electrolysis. J Electrochem Soc 2021;168:014510. https://doi.org/10.1149/1945-7111/abda57.

[26] Haug P, Koj M, Turek T. Influence of process conditions on gas purity in alkaline water electrolysis. Int J Hydrogen Energy 2017;42:9406–18. https://doi.org/10.1016/j.ijhydene.2016.12.111.

[27] Lee HI, Mehdi M, Kim SK, Cho HS, Kim MJ, Cho WC, et al. Advanced Zirfon-type porous separator for a high-rate alkaline electrolyser operating in a dynamic mode. J Membr Sci 2020;616:118541. https://doi.org/10.1016/j.memsci.2020.118541.

[28] Brauns J, Turek T. Experimental evaluation of dynamic operating concepts for alkaline water electrolyzers powered

by renewable energy. Electrochim Acta 2022;404:139715. https://doi.org/10.1016/j.electacta.2021.139715.
[29] Schalenbach M, Tjarks G, Carmo M, Lueke W, Mueller M, Stolten D. Acidic or alkaline? Towards a new perspective on the efficiency of water electrolysis. J Electrochem Soc 2016;163:F3197–208. https://doi.org/10.1149/2.0271611jes.
[30] Barthels H, Brocke WA, Bonhoff K, Groehn HG, Heuts G, Lennartz M, et al. PHOEBUS-Jülich: an autonomous energy supply system comprising photovoltaics, electrolytic hydrogen, fuel cell. Int J Hydrogen Energy 1998;23:295–301. https://doi.org/10.1016/s0360-3199(97)00055-4.
[31] Ulleberg Ø. Modeling of advanced alkaline electrolyzers: a system simulation approach. Int J Hydrogen Energy 2003;28:21–33.
[32] Henao C, Agbossou K, Hammoudi M, Dubé Y, Cardenas A. Simulation tool based on a physics model and an electrical analogy for an alkaline electrolyser. J Power Sources 2014;250:58–67. https://doi.org/10.1016/j.jpowsour.2013.10.086.
[33] Ursúa A, Sanchis P. Static-dynamic modelling of the electrical behaviour of a commercial advanced alkaline water electrolyser. Int J Hydrogen Energy 2012;37:18598–614. https://doi.org/10.1016/j.ijhydene.2012.09.125.
[34] Gilliam RJ, Graydon JW, Kirk DW, Thorpe SJ. A review of specific conductivities of potassium hydroxide solutions for various concentrations and temperatures. Int J Hydrogen Energy 2007;32:359–64. https://doi.org/10.1016/j.ijhydene.2006.10.062.
[35] Nickel Institute. Alloy selection for service in caustic soda. A guide to the use of Nickel-containing alloys. 2019.
[36] Fischer UR, Voigt A, Tannert D, Krautz HJ. Pressure and temperature influence on alkaline water electrolysis performance. Eur. PEFC H2 forum; 2015.
[37] Fischer UR, Voigt A, Tannert D, Krautz HJ. Alkaline pressure electrolysis-advantages and disadvantages. 21th world hydrog. Energy Conf.; 2016.
[38] Abdin Z, Webb CJ, Gray EMA. Modelling and simulation of an alkaline electrolyser cell. Energy 2017;138:316–31. https://doi.org/10.1016/j.energy.2017.07.053.
[39] Jang D, Cho HS, Kang S. Numerical modeling and analysis of the effect of pressure on the performance of an alkaline water electrolysis system. Appl Energy 2021;287. https://doi.org/10.1016/j.apenergy.2021.116554.
[40] Olivier P, Bourasseau C, Bouamama PB. Low-temperature electrolysis system modelling: a review. Renew Sustain Energy Rev 2017;78:280–300. https://doi.org/10.1016/j.rser.2017.03.099.
[41] Hammoudi M, Henao C, Agbossou K, Dubé Y, Doumbia ML. New multi-physics approach for modelling and design of alkaline electrolyzers. Int J Hydrogen Energy 2012;37:13895–913. https://doi.org/10.1016/j.ijhydene.2012.07.015.
[42] LeRoy RL. Industrial water electrolysis: present and future. Int J Hydrogen Energy 1983;8:401–17. https://doi.org/10.1016/0360-3199(83)90162-3.
[43] Li Z, Pitzer KS. Thermodynamics of aqueous KOH over the full range to saturation and to 573 K. J Solut Chem 1996;25:813–23. https://doi.org/10.1007/BF00972574.
[44] O'Brien T, Bommaraju TV, Hine F. Handbook of chlor-alkali technology. Springer; 2005.
[45] Müller J, Lohrberg K, Wüllenweber H. Raney-Nickel-beschichtete elektroden. Chem Ing Tech 1980;52:435–6.
[46] Wendt H, Plzak V. Electrocatalytic and thermal activation of anodic oxygen- and cathodic hydrogen-evolution in alkaline water electrolysis. Electrochim Acta 1983;28:27–34. https://doi.org/10.1016/0013-4686(83)85083-X.
[47] Haverkort JW, Rajaei H. Voltage losses in zero-gap alkaline water electrolysis. J Power Sources 2021;497:229864. https://doi.org/10.1016/j.jpowsour.2021.229864.
[48] Schalenbach M, Lueke W, Stolten D. Hydrogen diffusivity and electrolyte permeability of the Zirfon PERL separator for alkaline water electrolysis. J Electrochem Soc 2016;163:F1480–8. https://doi.org/10.1149/2.1251613jes.
[49] Hnedkovsky L, Bochmann S, May PM, Hefter G. Molar volumes and heat capacities of aqueous solutions of potassium hydroxide and for water ionization up to 573 K at 10 MPa. J Chem Eng Data 2017;62:2959–72. https://doi.org/10.1021/acs.jced.7b00192.
[50] Novotný P, Söhnel O. Densities of binary aqueous solutions of 306 inorganic substances. J Chem Eng Data 1988;33:49–55. https://doi.org/10.1021/je00051a018.
[51] LeRoy RL, Bowen CT, LeRoy DJ. The thermodynamics of aqueous water electrolysis. J Electrochem Soc 1980;127:1954–62. https://doi.org/10.1149/1.2130044.
[52] Allebrod F. High temperature and pressure alkaline electrolysis. Technical University of Denmark; 2013.
[53] Knaster MB, Apelbaum LA. Solubility of hydrogen and oxygen in concentrated potassium hydroxide solution. Russ J Phys Chem 1964;38:223–5.
[54] Tjaden B, Brett DJL, Shearing PR. Tortuosity in electrochemical devices: a review of calculation approaches. Int Mater Rev 2018;63:47–67. https://doi.org/10.1080/09506608.2016.1249995.
[55] MacMullin RB, Muccini GA. Characteristics of porous beds and structures. AIChE J 1956;2:393–403. https://doi.org/10.1002/aic.690020320.
[56] Tham MK, Walker RD, Gubbins KE. Diffusion of oxygen and hydrogen in aqueous potassium hydroxide solutions. J Phys Chem 1970;74:1747–51. https://doi.org/10.1021/j100703a015.
[57] Vogt H. On the supersaturation of gas in the concentration boundary layer of gas evolving electrodes. Electrochim Acta 1980;25:527–31. https://doi.org/10.1016/0013-4686(80)87052-6.
[58] Vogt H. The quantities affecting the bubble coverage of gas-evolving electrodes. Electrochim Acta 2017;235:495–9. https://doi.org/10.1016/j.electacta.2017.03.116.
[59] Shibata S. The concentration of molecular hydrogen on the platinum cathode. Bull Chem Soc Jpn 1963;36:53–7. https://doi.org/10.1246/bcsj.36.53.
[60] Lu Z, Zhang L, Iwata R, Wang EN, Grossman JC. Transport-based modeling of bubble nucleation on gas evolving electrodes. Langmuir 2020;36:15112–8. https://doi.org/10.1021/acs.langmuir.0c02690.
[61] Trinke P, Bensmann B, Hanke-Rauschenbach R. Current density effect on hydrogen permeation in PEM water electrolyzers. Int J Hydrogen Energy 2017;42:14355–66. https://doi.org/10.1016/j.ijhydene.2017.03.231.
[62] Agfa. Technical data sheet ZIRFON UTP 220 product description. 2021.
[63] Schug CA. Operational characteristics of high-pressure, high-efficiency water hydrogen-electrolysis. Int J Hydrogen Energy 1998;23:1113.
[64] Abe I, Fujimaki T, Matsubara M, Yokoo Y. Hydrogen production by high-temperature, high-pressure water electrolysis III: results of 80 kW pilot plant operation. Adv Hydrogen Energy 1984;2:727–36.
[65] Srinivasan S, Salzano FJ. Prospects for hydrogen production by water electrolysis to be competitive with conventional methods. Int J Hydrogen Energy 1977;2:53–9. https://doi.org/10.1016/0360-3199(77)90066-0.
[66] de Jonge RM, Barendrecht E, Janssen LJJ, van Stralen SJD. Gas bubble behaviour and electrolyte resistance during water electrolysis. Int J Hydrogen Energy 1982;7:883–94. https://doi.org/10.1016/0360-3199(82)90007-6.
[67] Heraldsen K, Leth-Olsen H. Stress-corrosion cracking of stainless steels in high pressure alkaline electrolysers. First Int. Conf. Hydrog. Saf.; 2005. p. 95–134. https://doi.org/10.31399/asm.tb.sccmpe2.t55090095.